Chapter 14

Graphene Cold Field-Emission Sources for Electron Microscopy Applications

Anjam Khursheed and Xiuyuan Shao
Department of Electrical and Computer Engineering,
National University of Singapore, Singapore 117576, Singapore
eleka@nus.edu.sg, eleshao@nus.edu.sg

The theoretical and experimental emission characteristics of the room-temperature field-emission source are reviewed as they relate to scanning electron microscopy, transmission electron microscopy, and scanning transmission electron microscopy applications. A brief history of the development of the cold-field electron source is given. Work function, energy distribution, source electron optics, and current fluctuations are the main source characteristics considered. The general focus of this chapter is on the newly developed single-crystal graphene coated nickel cold field-emission sources.

14.1 Introduction

The emission of electrons being emitted from a sharply pointed cold metal surface under the presence of a strong electric field, a

Nanostructured Carbon Electron Emitters and Their Applications
Edited by Yahachi Saito
Copyright © 2022 Jenny Stanford Publishing Pte. Ltd.
ISBN 978-981-4877-62-6 (Hardcover), 978-1-003-14199-0 (eBook)
www.jennystanford.com

process called "field emission (FE)," was first reported by Robert Williams Wood, in 1897 [1]. A potential barrier is established by the potential step at the metal surface confining the electrons to the solid, which is to a first approximation, triangular in shape. The height of the potential barrier is given by the work function of the solid. The first clear picture of the FE mechanism in terms of the newly developed theory of quantum mechanics was developed by Fowler and Nordheim in 1928 [2]. Under the influence of a high electric field, the width of the potential barriers becomes thinner and the electrons close to the Fermi level have a finite probability to tunnel through the barrier and escape. In the early 1960s, many of the successful investigations of field-emission phenomena came from three groups led by Professors Erwin Muller (Pennsylvania State University), Robert Gomer (University of Chicago), and Walter Dyke (Linfield College and Linfield Research Institute) [3–5]. Dyke and coworkers proposed a variety of applications of a cold field-emission (CFE) source and formed the first company to produce CFE-based commercial products. The successful application of CFE cathodes to electron microscopy, including both scanning electron microscopy (SEM) and scanning transmission electron microscopy (STEM), was achieved by a group led by Professor Albert Crewe at the Enrico Fermi Institute in Chicago in the late 1960s [6, 7].

A locally high electric field needs to be created for FE to take place, which requires the field emitting tip to have large field enhancement factors. For the past half a century, a great variety of refractory metals, semiconductors, nanowires, single-atom tips, and a variety of nanotips have been investigated for their FE properties [8–10]. The investigations and developments of CFE electron sources turned out to be quite discouraging by the fact that CFE electron sources are found to be not very stable and reliable. For over 40 years, the most common type of CFE electron source used in high-resolution microscopy utilizes a single crystal (310)-oriented tungsten-sharpened wire as the cathode, whose tip radius is in the 100–200 nm range with a work function (ϕ) of 4.4 eV [11]. Typically, electron emission from the cathode occurs when the field strength at the cathode tip exceeds values around 4 V/nm for single-crystal tungsten, allowing electrons to escape from the cathode surface by quantum tunneling. However, single-crystal tungsten CFE sources suffer from some practical engineering problems that have limited their widespread use. One difficulty comes from the native oxide

material that forms on the cathode surface and subsequently quenches electron emission, requiring the use of ultrahigh vacuum (UHV) levels in the gun unit ($<10^{-10}$ Torr). Even at such stringent vacuum conditions, the intensity of electron emission falls in 1 to 2 h of continuous operation and the cathode needs to be warmed or rapidly heated (flashed to ~2000 K) regularly to blow off material. One disadvantage of this flashing process is that it will interrupt the continuous operation of the electron beam instruments. Recently, Hitachi has developed a "Mild flashing" technology for their latest generation of CFE source SEMs, which is executed automatically in the background to gently clean the FE source at regular intervals while maintaining a high voltage [12]. This technology enables stable and continuous operation of the new CFE source. However, the feasibility of using this technology requires extreme-stringent UHV conditions ($\sim 10^{-12}$ Torr), and this will be a challenge for many practical electron beam applications.

Since the discovery of two-dimensional (2D) graphene in 2004, graphene has attracted much attention as a potential candidate for CFE source emitters, due to its high aspect ratio (the lateral size to the thickness) and excellent thermal, mechanical, and electrical properties [13]. Excellent field emission from graphene has been demonstrated from a wide variety of different microfabricated structures, and most of them consist of densely packed nano-emitters that produce a large array of defocused overlapping electron beams, and therefore cannot be subsequently defocused down to a single nanometer electron probe [14–16]. For an FE electron source to be useful for high-resolution electron optical instruments, it must have its dominant emission direction on the optical axis, be stable over a sufficient long period of time, and be resistant to different types of current fluctuations in practical vacuum environments.

14.2 Work Function

The key parameter that determines the highest achievable brightness with the lowest energy spread of a CFE point-cathode electron source is the low work function of the emitting material. For electron microscopy applications, as electrons are accelerated through the gun unit, the wide-angle ones are filtered out by the first, second anode plate holes and gun apertures, and they exit the gun unit in the form of a rotationally symmetric electron beam that

appears to emanate from a single point on the axis. This single point on the axis, known as virtual source, is defined as the spot at which the back-projected trajectories of emitted electrons are focused. The relatively small virtual source size of CFE guns (a few nanometers in diameter) is one of the main reasons for them having the highest brightness of all electron sources used in focused electron beam instruments. In fact, only a small portion of the beam current contained in a small solid angle centered at the emitter axis is useful. Therefore, the state-of-the-art single-crystal tungsten-sharpened wire needs to be etched in a specific plane (such as the <310> plane) to generate the lowest work function on the apex of the tip, in order to have sufficient emission for a small acceptance aperture centered on the emitter axis.

Graphene is well known for possessing several desirable properties: (1) it has excellent thermal, mechanical, and electrical characteristics [17, 18]; (2) its work function can be significantly lowered both by direct contact with metals (effectively doping it) and through the application of intense electric fields [19, 20]; and (3) it is extremely flexible. Recent progress shows that the characteristic electronic structure of graphene can be significantly altered by chemisorption on metal substrates, resulting in doping either with electrons or holes. The work function (ϕ) of graphene can be reduced to as low as 3.66 eV when chemisorbed on Ni (111). Fast development of 2D graphene in recent years has led to a variety of graphene-based FE electron sources, including graphene film emitters, graphene point/edge-cathode emitters, and graphene ring-cathode emitters [21]. However, none of these graphene sources has yet been utilized for commercial high-resolution electron beam instruments.

Recently, the research group at the National University of Singapore, led by A. Khursheed, have presented the development of a completely new type of CFE electron source, a Graphene–Ni (Gr–Ni) point cathode for electron microscopy systems [22]. One of the standout features of the Gr–Ni point cathodes reported in their work are ultralow work function values (~1.1 eV), as evidenced in Fig. 14.1. The work function for the Gr–Ni CFE source is determined by using two Fowler–Nordheim (F–N) plots, one for the bare Ni tip and the other for the graphene-coated Ni tip, and then by taking the ratio of their F–N slopes, eliminating the anode–cathode separation d and field-enhancement factor β. This procedure assumes that the

addition of graphene does not change the tip geometry (confirmed by SEM imaging). From the ratio of the two F–N slopes, the effective work function is calculated from:

$$\phi_{\text{Graphene+Ni}} = \phi_{\text{Ni}} \sqrt[1.5]{\left(\frac{m_{\text{Graphene+Ni}}}{m_{\text{Ni}}}\right)}, \tag{14.1}$$

where $\phi_{\text{Graphene+Ni}}$ and ϕ_{Ni} are the work functions of graphene-coated and bare Ni-pointed cathodes, respectively, while $m_{\text{Graphene+Ni}}$ and m_{Ni} are the slopes of their respective F–N plots.

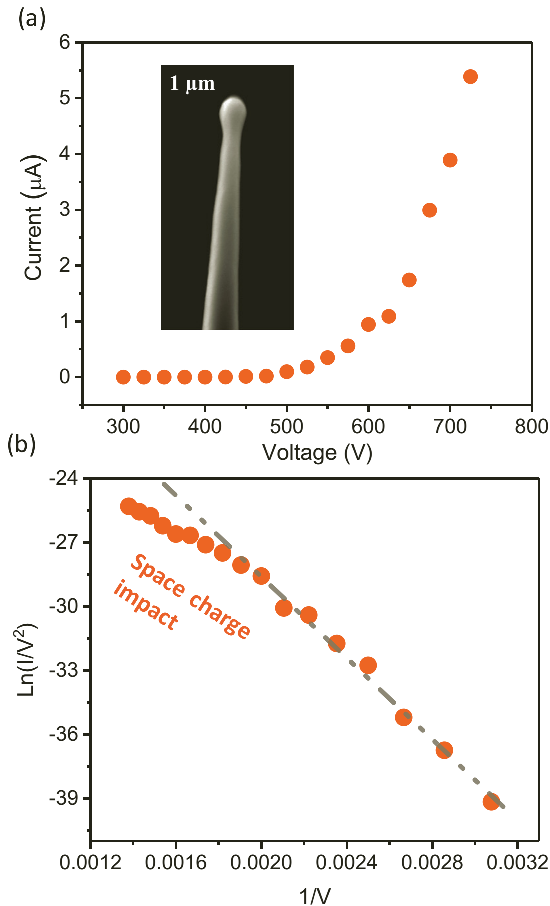

Figure 14.1 Field electron emission characteristics from a Ni tip with a tip radius of 500 nm after coating with graphene, with an anode–cathode spacing of 0.5 mm.

14.3 Energy Distribution

14.3.1 Theoretical Background

The energy spread (ΔE), through the chromatic aberration of the objective lens, degrades the final spatial resolution of an electron optical system, particularly at high relative beam energy spreads. Ideally, the energy distribution of the emitted electron beam should be as narrow as possible while maintaining sufficient brightness. The energy distribution is a convolution of an intrinsic contribution, determined solely by the properties of the material of the emitting surface and extrinsic contributions. An analytical expression for the intrinsic energy distribution (known as total energy distribution (TED)) of electron emission in the thermal field regime was first derived by Young [23] based on the free-electron model as:

$$P(E) = \frac{J_{\mathrm{FN}}}{d}\left[\frac{\exp\left(\frac{E-E_f}{d}\right)}{1+\exp\left(\frac{E-E_f}{kT}\right)}\right], \tag{14.2}$$

where kT = 25.9 meV at 300K, J_{FN} is the F–N emission current density formula developed by Murphy and Good (later modernized), and d is the tunneling parameter (in eV) given by:

$$d = (2/3b)\, t^{-1}(y)\, \phi^{-1/2} F$$

$$(2/3b) = 9.76 \times 10^{-11} \quad [\mathrm{eV}^{3/2}\,\mathrm{V}^{-1}\,\mathrm{m}] \tag{14.3}$$

where F and ϕ are the electric field strength (in V/m) and the work function (in eV), b is the 2nd F–N constant, and $t(y)$ is a slowly varying function of $y = 3.79 \times 10^{-5} F^{1/2}/\phi$ and can be approximated by the formula $t(y) = 1 + 0.1107y^{1.33}$. The analytical formula is valid provided $kT/d < 0.7$ and $y < 1$ [24]. Figure 14.2 shows the room temperature TED for a typical W(310) cold field emitter at ϕ = 4.32 eV and F = 4.34 V/nm as well as for a Gr–Ni tip at ϕ = 1.10 eV and F = 0.781 V/nm. From these plots, the intrinsic full-width at half-maximum (FWHM) energy spreads are calculated to be 0.23 and 0.14 eV, respectively. The smaller predicted intrinsic FWHM of the Gr–Ni cathode compared to the typical W(310) CFE source comes mainly from its smaller field strength requirement.

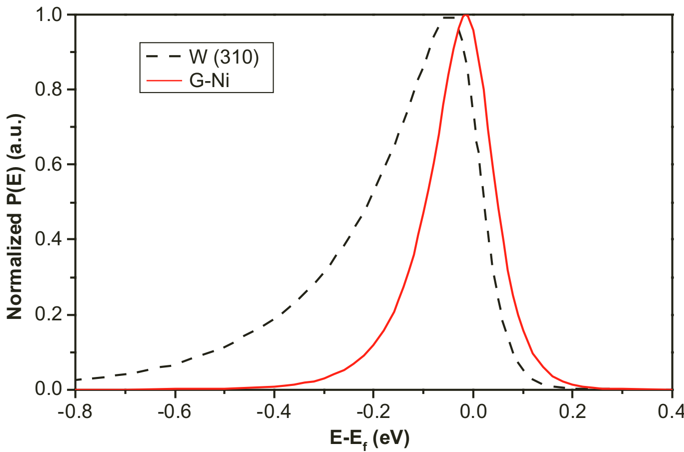

Figure 14.2 Room temperature intrinsic energy distributions for a typical W(310) cold field emitter (ϕ = 4.32 eV, F = 4.34 V/nm) and a Gr–Ni emitter (ϕ = 1.10 eV, F = 0.781 V/nm). The FWHM energy spreads are 0.23 and 0.14 eV, respectively.

14.3.2 Statistical Coulomb Interactions

Charged particle optics is made possible by the fact that trajectories of charged particles are shaped and influenced by electrostatic and magnetic field distributions, this makes it possible to design and make electron lenses and deflectors. However, it also means that the trajectories of electron beams are also affected by statistical coulomb effects, caused by the mutual electrostatic repulsion force between neighboring electrons in the beam. These statistical coulomb interactions manifest as energy broadening or more commonly known as Boersch effect (due to longitudinal interactions) and the trajectory displacement effect (due to lateral interactions), and thus degrades the quality of an electron beam's optical properties [25]. The former adds to the intrinsic source energy spread while the latter causes an additional enlargement of the virtual source size which effectively reduces the source brightness. These two statistical coulomb effects can be estimated in an approximate way by Monte Carlo numerical simulations, and also by simple analytical approximations [26, 27].

The energy broadening, representing the change in axial velocity, was firstly found and investigated by Boersch using a thermionic cathode in 1954 [25]. It has been further experimentally verified for point-cathode FE sources by Bell and Swanson in 1979 [28]. The Boersch effects can be approximated by analytical equations for different regimes of the beam, including Gaussian, Holtsmark, Lorentzian, and the pencil beam regime [27]. For the gun section, the electrons are assumed to be accelerated to V_{ext} in the whole gun segment, the appropriate regime is the Holtsmark regime, and the contribution to the apparent source size is (given by Knauer) [26]:

$$\Delta E_{\text{Boersch}} = 15.9 \frac{(I')^{2/3}}{r_{\text{tip}}^{1/3} V_{\text{ext}}^{1/3}}, \tag{14.4}$$

where I' is the emitted angular current density, r is the emitter radius, and V is the beam voltage.

Usually, to a first approximation, the energy broadening term is added in quadrature with the intrinsic emission energy distribution width term to obtain the total beam energy width:

$$\Delta E_{\text{total}} = \left(\Delta E_{\text{intrinsic}}^2 + \Delta E_{\text{Boersch}}^2\right)^{1/2}. \tag{14.5}$$

Predictions using these equations for a conventional W(310) electron source and different diameter tip Gr–Ni electron sources are shown in Table 14.1.

For the smaller tip sizes, the smaller energy spreads expected for the Gr–Ni cathode (using typical parameters from Gr–Ni) compared to conventional tungsten CFE sources (of comparable tip size) based upon the TED distribution will be approximately offset by the Boersch effect. It is interesting to note that since both the TED distribution and Boersch effect on energy spread decrease with increasing tip radius, a significantly smaller energy spread is predicted for the 800 nm radius Gr–Ni tip (a factor of 2 smaller than that of the 170 nm radius tip). This would ordinarily not be possible for conventional large field emitters (tip diameters over 1 μm), such as the Schottky emitter, since the Schottky field emitter only functions by heating the tip up to 1800 K, enlarging the energy spread by thermal effects to around 0.5 eV.

Table 14.1 Energy spread predicted by semianalytical calculations

Source	r_{tip} (nm)	V_{ext} (V)	I' (μA/sr)	d_v (nm)	B_r (A/m^{2}srV)	$\Delta E_{intrinsic}$ (eV)	$\Delta E_{Boersch}$ (eV)	ΔE_{total} (eV)
W(310)	160	4255	62	2.98	2.09×10^9	0.232	0.283	0.366
Gr–Ni	170	975	40.7	4.55	2.51×10^9	0.144	0.342	0.371
Gr–Ni	400	1300	45.5	8.27	7.09×10^8	0.140	0.252	0.288
Gr–Ni	800	1450	11.4	11.79	7.23×10^7	0.136	0.077	0.156

The trajectory displacement effect (Radial broadening), first investigated by Loeffler in 1964, represents the lateral shift in a particle's position and a change in the velocity component perpendicular to the beam axis [29]. A "slice method" can be used to calculate the trajectory displacement, in which the region to be calculated is divided into small segments, where the beam voltage and size is assumed to remain constant within each segment [30]. The trajectory displacement is calculated by applying the slice method to an analytical approximation in the gun region.

$$d_{\text{blur}} = \int \frac{l(z)}{M(z)} \phi_{\text{J}}(r(z), V(z), I)\, dz, \tag{14.6}$$

where $l(z) = r(z)/a(z)$ and $M(z)$ is the magnification $\left(= \left(\frac{\alpha_{ref}}{\alpha(z)}\right)\sqrt{\left(\frac{V_{ref}}{V(z)}\right)} \right)$.

The slice method requires the angular displacement per meter, given by:

$$\phi_{\text{J}} = \left[\frac{T_1 D_\lambda^{18/7} D_{\text{r}}^6 I^{18/7} r^{6/7} V^{-15/7}}{T_4 + T_2^{1/7} D_{\text{r}}^6 D_\lambda^2 I^2 r^2 V^{-1}} \right]^{7/6}, \tag{14.7}$$

where $D_\lambda = m^{1/2} / (\pi 2^{7/2} \epsilon_0 e^{1/2})$ and $D_{\text{r}} = \left(\frac{2\epsilon_0 \pi}{e}\right)^{1/3}$. The constants are $T_1 = 4.618 \times 10^{-2}$, $T_2 = 2.041 \times 10^5$, and $T_4 = 6.25 \times 10^{-2}$. $V(z)$ and $r(z)$ are determined using numerical field solving and ray-tracing simulations. One example of this is shown in Fig. 14.3.

The integration is done with Simpson's 1/3 rule applied to unequal intervals. Radial broadening has the effect of increasing the intrinsic virtual source size d_{v}, which in turn will lower the brightness estimate by a correction factor K given by:

$$K = \frac{d_v^2}{d_v^2 + d_{\text{blur}}^2}, \tag{14.8}$$

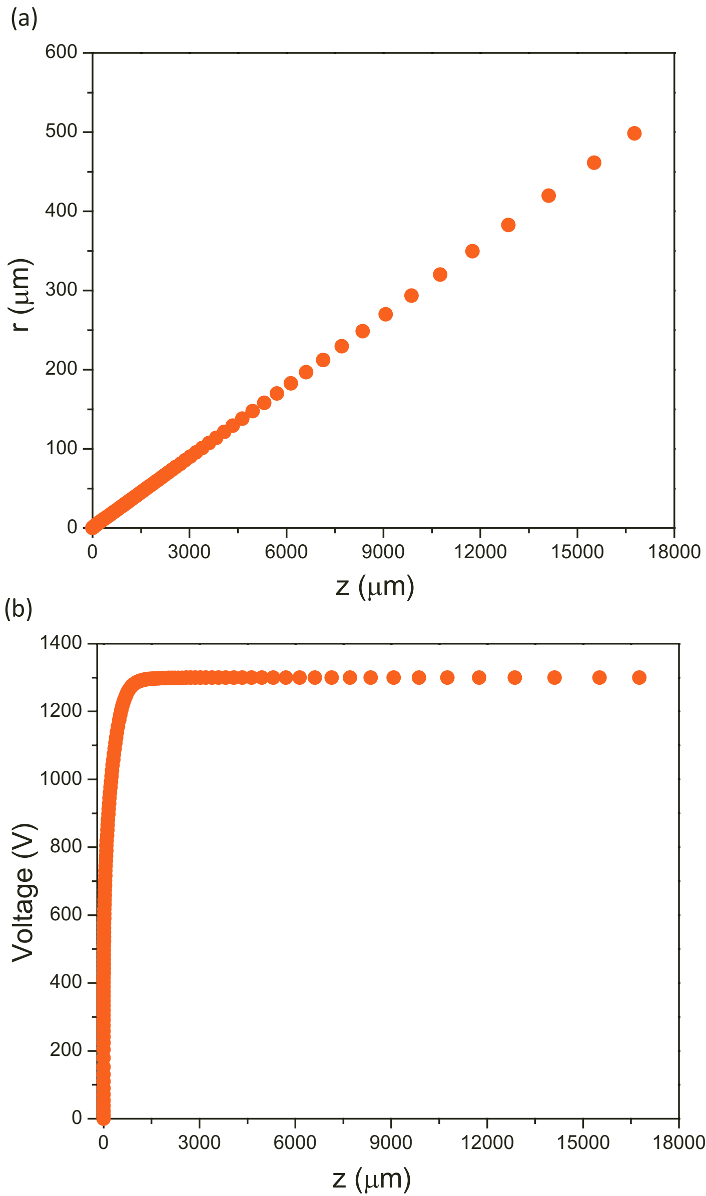

Figure 14.3 (a) Beam radius versus axial distance and (b) potential versus axial distance for trajectory displacement calculation.

14.3.3 Measured Values of the FWHM Energy Spread for the Graphene Cold Field Electron

The measured energy distribution is a convolution of several different effects. They include: (i) the intrinsic energy distribution, (ii) the Boersch effect, and (iii) the finite energy resolution of the analyzer. If the cathode current density is maintained to be relatively low and the resolution of the analyzer is high, the Boersch effect is minimized and the electron beam contains only the energy distribution from the emission process. Figure 14.4 shows the measured beam intensity with respect to electron kinetic energy from the Gr–Ni CFE source at different pass energies for a tip diameter of 200 nm. An upper bound to the energy spread is approximately given by the lowest pass energy value, since the energy resolution of the energy analyzer varies linearly with pass energy value. The overall energy spread values are lower than or comparable with state-of-the-art conventional CFE sources, which is ordinarily not possible for conventional large-size FE electron sources, such as the Schottky emitter, since the Schottky FE source only functions by heating the tip up to 1800 K, enlarging the energy spread by thermal effects to around 0.5 eV. The low energy spread is of particular importance since chromatic aberration of the objective lens is the main factor limiting spatial resolution.

For electron optical analysis, measurement of the beam energy distribution does not have any practical meaning without the simultaneous measurement of the cathode current density J_{FN}. There is a relationship between J_{FN} and angular current density I' with apex radius r, and is useful, since I' is more easily measured. The relationship is given by [31]:

$$I' = J_{FN}\left(\frac{r}{m_{\alpha}}\right)^{2}, \tag{14.9}$$

where m_{α} is the angular magnification. Trajectory ray-tracing simulation needs to be used to compute the exact value of angular magnification $m_{\alpha} = \alpha/\theta$, where α is the final extraction angle (limited by a small acceptance aperture) and θ is the initial emission angle. The simulated m_{α} is found to lie between 0.5 and 0.7, depending on details of the emitter shape. Alternatively, the cathode current

density can be directly calculated by simulating the cathode emission area S_p. By using a Faraday cup with a small acceptance aperture (restricting the semiangle entry to say 30 mrad), the emission current can be traced back to a small cathode emission area S_p. For tip radii in the range of 130–800 nm, S_p was estimated to be in the range of 130–3965 nm^2. The detailed relationship between electron energy distribution and angular current density I' for Gr–Ni electron sources will be discussed in the next section.

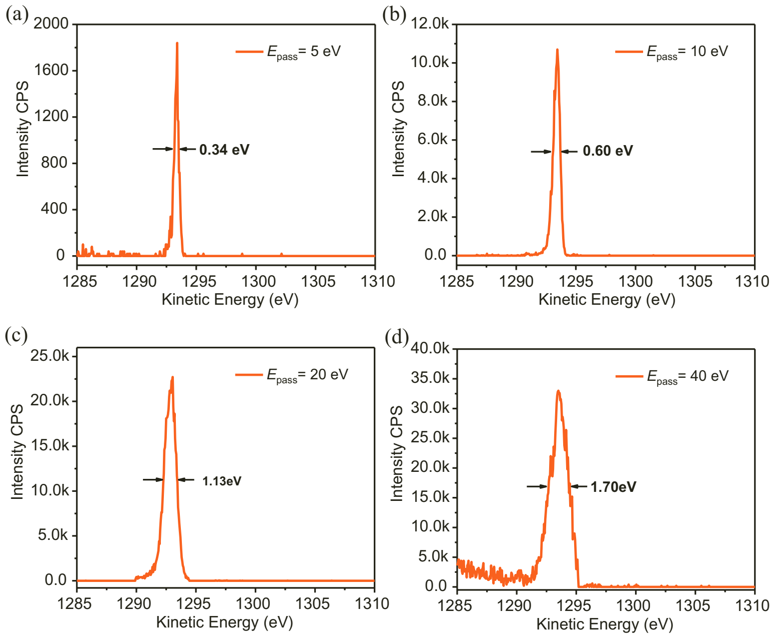

Figure 14.4 Measured FWHM values with different pass energies (5–40 eV) for a tip diameter of 200 nm measured by a cylindrical sector analyzer (CSA 200).

14.4 Source Electron Optics

For successful electron microscopy applications, a high source brightness (B_r) and a low energy spread (ΔE) are always needed to provide a high-resolution focused electron beam. The calculation of B_r requires knowledge of the virtual source size (d_v), defined to be the waist of the crossover formed by the back projection towards the

emitter from tangents to the exit electron trajectories. It is given by the following expression [32]:

$$B_r = \frac{4I'}{\pi d_v^2 V_{ext}}, \tag{14.10}$$

where I' is the angular current density, d_v is the virtual source size, and V_{ext} is the extraction voltage. The virtual source size can be calculated using the formula:

$$d_v = 1.67 \frac{r_{tip}}{m_\alpha} \sqrt{\frac{< E_t >}{eV_{ext}}}, \tag{14.11}$$

where r_{tip} is the tip radius and $< E_t >$ is defined as $< E_t > = e\hbar F/\sqrt{(8m\phi)}$, with F the local electric field, ϕ the work function, and $\hbar$ the reduced Planck constant. After simplification, the source-reduced brightness for CFE electron sources is given by:

$$B_r = 1.44 \frac{eI'}{\pi < E_t >} \left(\frac{m_\alpha}{r_{tip}} \right)^2. \tag{14.12}$$

For high brightness electron beam applications, statistical Coulomb interactions lead to radial broadening of the virtual source size due to lateral electron–electron interactions, which in turn lowers the practical reduced brightness. It should be noted that the analytical method just outlined avoids the need to measure the virtual source diameter d_v experimentally, and this is important, because direct measurements of the virtual source diameter are not trivial.

Figure 14.5a presents semianalytically calculated B_r values for graphene-coated point cathodes versus tip radii, together with state-of-the-art FE electron sources. The data in the plot can be broadly grouped into three categories: high brightness tungsten CFE electron sources with very small tip radii (<200 nm) [11, 33], Schottky emitters having relatively low brightness with large tip radii (~1000 nm) [33, 34], and Gr–Ni CFE electron sources having tip dimensions that roughly fall in the middle region. The estimated B_r value of 2.51×10^9 A/m^{2}srV of a graphene-coated cathode of tip radius 170 nm is very close to the highest reported B_r value of 3.98×10^9 A/m^{2}srV for a conventional tungsten cold field W(310) emitter with a tip radius of 160 nm. When corrected with the trajectory displacement effect (via Eq. (14.1.8)), the brightness

will be lowered by Coulomb interaction effect significantly for the smaller Gr–Ni cathode tip radius (reduction by around 30% for the 170 nm tip radius) and is not expected to significantly lower the brightness estimates for the larger Gr–Ni cathode tip radii. The I' can be easily obtained by dividing the beam current over the solid angle defined by the beam acceptance aperture. With the simultaneous measurement of the electron energy distribution, the reduced brightness versus energy spread is plotted in Fig. 14.5b. The overall energy spread values are lower than or comparable with state-of-the-art conventional CFE sources.

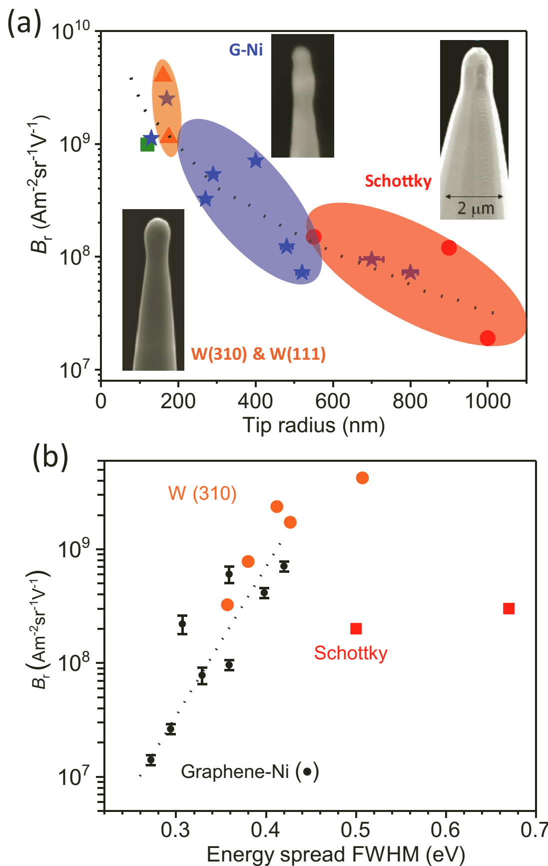

Figure 14.5 (a) Comparison of reduced brightness to the state-of-the-art FE electron sources (Yellow triangle: W(310) [11, 33]; Green square: W(111) [33]; Red circle: Schottky sources [33, 34]; and Blue star: Gr–Ni sources). (b) Reduced brightness versus energy spread and state-of-the-art electron sources.

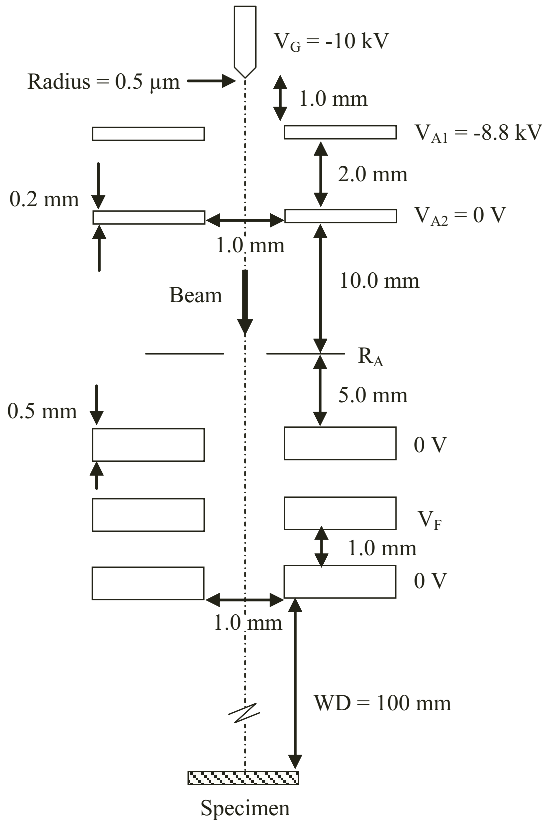

Figure 14.6 Schematic diagram for a 10-kV test column designed to measure the virtual size experimentally.

Figure 14.6 shows the schematic diagram of a 10-kV test column that can be used to determine the practical virtual source size d_v experimentally. Simulation has been done to obtain the optimum values for the final aperture radius R_A for a 100-mm working distance with an accelerating Einzel lens for a high (10-kV) beam voltage. The optimal aperture radius here gives the probe radius that is dominated by the virtual source size contribution. In the test column, the total beam size in the image plane is limited by spherical aberration d_s, diffraction d_l, and virtual source size d_v. Chromatic aberration is negligible (e.g., $C_\mathrm{C}(\Delta E/E)\alpha$ = 6 nm for ΔE = 0.2 eV at R_A = 15 μm) and hence not shown. The probe radius–aperture radius relation (shown in Fig. 14.7) is calculated for the 10-kV beam voltage

using the Barth-Kruit formula with C_S = 6249.415 m and C_C = 1.540 m. For the 10-kV test column, at the optimum R_A = 15 μm, the middle Einzel lens voltage is V_F = 6625.4 V, giving a magnification factor of M = 4.5. The virtual source radius is 15 nm (F = 0.6 V/nm and m_α = 0.16 predicted and take ϕ = 2 eV), giving a source image radius of 68 nm, while the spherical aberration radius and diffraction radius are minimized to be 11 and 18 nm, respectively.

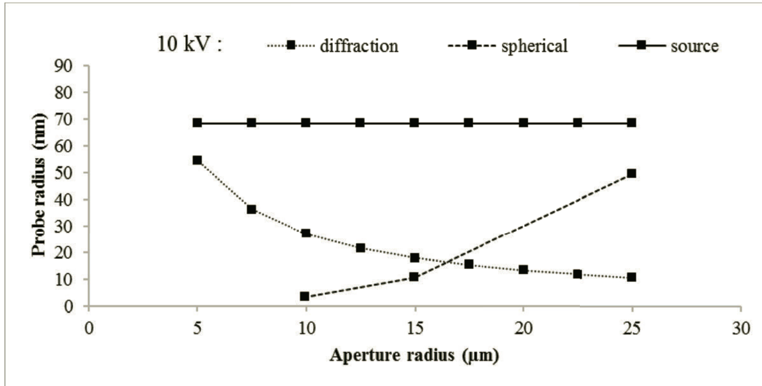

Figure 14.7 Predicted probe diameter for 10-kV beams as a function of final aperture radius. In this plot, spherical aberration is calculated as the RMS radius at the least-confusion plane. Chromatic aberration is ignored since it is negligible.

14.5 Current Fluctuations

14.5.1 Short-Term Current Fluctuations

The stability of the electron beam is of major concern for focused electron beam applications. By ignoring the preexponential term, the Murphy–Good version of F–N theory can be used to show

$$\frac{\delta I}{I} = -\frac{\delta\phi}{d} = -\left[\frac{3b}{2t(y)}\right](\phi^{1/2}\,\delta\phi)(\beta V)^{-1}. \qquad (14.13)$$

Therefore, the drift in ϕ and/or β in the emitting area will cause inevitable current fluctuations. Previous studies have shown that conventional CFE electron sources are prone to instability in practical vacuum environments due to [5, 11, 35]:

1. A $1/f$ type noise component, in the presence of adsorbed layers this noise becomes dominant.
2. A generation–recombination process on the cathode surface.
3. Shot noise, caused by uncertainties taking the form of a Poisson distribution, which describes the occurrence of independent random events.
4. Velocity fluctuations caused by the ion oscillations, also known as ion back-bombardment problems.

It has also been shown by L. W. Swanson that current fluctuations arise from the generation of mobile atoms on net plane terraces for single-crystal tungsten emitters [35]. One of the most important advantages of Gr–Ni point cathodes over the conventional metal CFE emitters is the chemical inertness of its carbon surface, which is less likely to adsorb residual gas molecules and is therefore obviously much more stable [36]. In addition, a lower turn-on electric field is desirable for CFE electron sources since it will reduce the kinetic energies up to which the back-bombarding gas-ions are accelerated to when they collide with the cathode surface. On the negative side, there are step jumps and spikes in the short-term beam current, which are always observed at low and moderate emission current densities for CFE electron sources with nanoscale emission area [37, 38]. The magnitude of these step jumps and spikes can sometimes be up to double the size of the preceding current, and the frequency of these step jumps and spikes can be as low as once in every tens of seconds. These step jumps and spikes can be significantly improved by improving the vacuum conditions, but they cannot be eliminated for the moment.

The degree of current instability and damage to the cathode tip depends not only on the chemical inertness of the carbon surface but also on the size of the cathode tip. It is theoretically predicted that the root mean square (RMS) noise ratio ($<\delta I^2>^{1/2}/\bar{I}$) varies inversely with the emission surface area, under constant conditions of temperature and pressure. Since for the same emission angle, a larger radius tip has a greater area of emission, the relatively large diameter graphene-coated cathode tips (in the micrometer range) are therefore expected to have an order of magnitude lower RMS noise ratio values as compared to conventional tungsten cold field emitters. The success of Schottky electron beam sources is primarily due to its large physical emitting surface area.

In electron beam noise measurements, the mean square noise power $<\delta I^2>$ is usually obtained, which is related to the well-known spectral density function $W(f)$ as follows:

$$\delta I^2_{f_1 \ldots f_2} = \int_{f_1}^{f_2} W(f)df \,, \qquad (14.14)$$

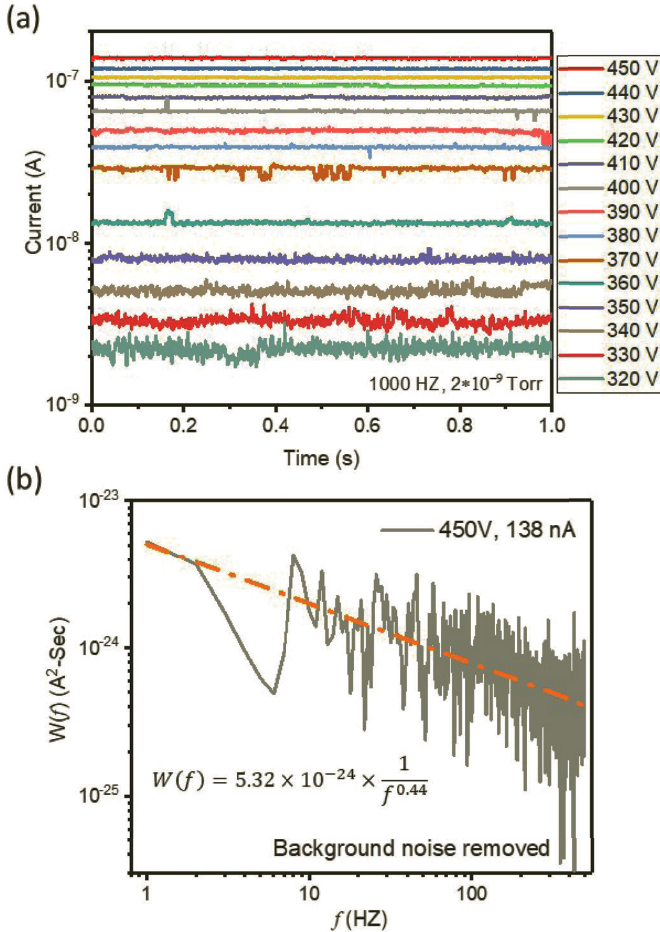

Figure 14.8 (a) Plot of current fluctuations from a graphene-coated Ni point-cathode CFE source at different extraction voltages with a sampling rate of 1000 Hz. (b) Power spectrum analysis of the probe current (138 nA) with a sampling rate of 1 kHz for a time span of 1 s.

Figure 14.8a presents a typical current–time trace from a Gr–Ni CFE source with a sampling rate of 1 kHz (a time span of 1 s), and the frequency dependence of $W(f)$, as defined in Eq. (14.13), is plotted in Fig. 14.8b. No flashing or other tip conditioning procedures were performed. An RMS noise ratio percentage, $\langle \delta I^2 \rangle^{1/2}/I = 0.576\%$, or a signal-to-noise ratio of 173.6 is obtained with a high measured current of 138 nA. The data also shows a $1/f$ roll off for $W(f)$, which was carried out for I = 138 nA at an extraction voltage of 450 V from a Gr–Ni CFE electron source. Due to the $1/f$ nature of the noise spectra, the emission noise is confined to the lower frequencies of the spectrum. The noise components at the high frequency part are entirely due to shot noise. This measured value is lower than that obtained from a conventional tungsten CFE emitter (2–5% at 10^{-10} Torr, $T = 25$ °C) [39], and is comparable to that obtained from CNT emitters (~0.2% at 6×10^{-8} Torr, $T = 500$ °C, $I = 2.4$ nA) [37] and Schottky emitters (~0.23% at 10^{-8} Torr, $T = 1527$ °C, $I = 30$ nA) [40] for the same frequency range.

14.5.2 Long-Term Current Drift

The failure to successfully apply many nanotips with promising electron optics performance to electron beam instruments is largely due to limitations in lifetime. The erratic and unstable performance in a UHV environment is caused by the sputtering effect from nanoscale emitting sites. Even for the successful commercial single-crystal tungsten CFE electron sources, the limitation in lifetime still exists. Their total emission current decays significantly (about 70–90% of the initial value) within the first hour of usage. Subsequently, regular cathode flashing (Joule heating at high temperatures) to blow-off the residual contaminant molecules at intervals as short as a few hours is required in order to reach original emission current levels. The following mechanisms given by Dyke's group may help explain the large long-term current drift [5]:

1. Localized changes in cathode work function, caused by the selective adsorption of electronegative gas such as oxygen, result in changes in the emission pattern and a decrease of total current with time.

2. Changes in β caused by deformation of the emitting surface. A surface projection tends to grow outward or extrude when either the temperature is high enough to cause appreciable surface migration or when surface atoms gain energy from ionic bombardment.

Later investigations by other researchers show that the ions formed near the emitter surface, and centered on the emitter axis, will impinge on the actual emitting area. Other ions generated from electron-stimulated desorption at the anode electrode will hardly be able to reach the emitting area. It was suggested that the ion bombardment effect will only dominate when $P \times I_t > 7 \times 10^{-12}$ *PaA* [41]. However, it should be noted that the energies of those ions impinging on the cathode are only ~10% of the inter-electrode electric potential (V_{ext}) [42]. Excessive ions may gather under a very high emission current around the emission surface and eventually trigger a catastrophic arc, which will end the life for the CFE source.

The long-term performance of the Gr–Ni CFE source has been studied for a sampling rate of 2 Hz in our lab. Before the long-term operation, the tip was carefully investigated under an SEM and a voltage–current measurement was carried out. No obvious current drift or decay was observed for Gr–Ni CFE sources, so thermal flashing is not required. The latest results show that the emission current from a Gr–Ni CFE source in UHV vacuum conditions is stable with no degradation over 6 months, which may be attributed to its ultralow work function and relatively low applied electric field strength at the tip apex. The structural robustness of Gr–Ni CFE sources against ion back-bombardment is confirmed by SEM characterizations.

14.6 Summary

High brightness, low energy spread, and good current stability are critical for CFE electron sources for electron microscopy applications. Although considerable research has been carried out into developing single-crystal tungsten and other nanotip CFE sources, they have as yet faced many practical technological difficulties, such as stringent UHV requirements, poor current stability, and short lifetime. This chapter highlighted some recent promising developments in the category of single-point Gr–Ni CFE electron sources for electron microscopy

applications. These current results establish the promising prospect of using them as high brightness high-resolution electron sources for electron microscopy and lithography applications, similar in performance to conventional single-crystal tungsten cathode CFE sources, while at the same time having better emission stability and less stringent vacuum requirements. However, the investigation of graphene-based CFE electron sources is still in an early stage of development, and there is still much room for further improvement. More emission characterization tests need to be performed, ones that can measure the source virtual source size, transverse coherent length, and emitter lifetime. Current fluctuations remain a practical challenge, and the mechanism of step jumps and spikes noises is not yet clear. An electron gun unit that can accommodate promising graphene emitters also needs to be developed in the future, which has its optical axis well aligned to the central axis of the cathode. Beyond that, electron guns based upon the new class of graphene-based field emitters need to be fitted on to electron microscopes, and their performance critically compared to conventional systems, in terms of parameters such as image resolution and signal-to-noise ratio.

References

1. R. W. Wood, "A new form of cathode discharge and the production of X-rays, together with some notes on diffraction. Preliminary communication," *Physical Review (Series I)*, vol. 5, no. 1, pp. 1–10, 1897.
2. R. H. Fowler and L. Nordheim, "Electron emission in intense electric fields," *Proceedings of the Royal Society of London. Series A, Containing Papers of a Mathematical and Physical Character*, vol. 119, no. 781, pp. 173–181, 1928.
3. R. H. Good and E. W. Müller, "Field emission," in *Electron-Emission Gas Discharges I/Elektronen-Emission Gasentladungen I*: Springer, pp. 176–231, 1956.
4. R. Gomer, "Current fluctuations from small regions of adsorbate covered field emitters: A method for determining diffusion coefficients on single crystal planes," *Surface Science*, vol. 38, no. 2, pp. 373–393, 1973.
5. W. Dyke and W. Dolan, "Field emission," in *Advances in Electronics and Electron Physics*, vol. 8: Elsevier, pp. 89–185, 1956.

6. A. Crewe, J. Wall, and L. Welter, "A high-resolution scanning transmission electron microscope," *Journal of Applied Physics*, vol. 39, no. 13, pp. 5861–5868, 1968.
7. A. V. Crewe, M. Isaacson, and D. Johnson, "A simple scanning electron microscope," *Review of Scientific Instruments*, vol. 40, no. 2, pp. 241–246, 1969.
8. H. Zhang et al., "An ultrabright and monochromatic electron point source made of a LaB 6 nanowire," *Nature Nanotechnology*, vol. 11, no. 3, pp. 273–279, 2016.
9. X. Shao, A. Srinivasan, Y. Zhao, and A. Khursheed, "A few-layer graphene ring-cathode field emitter for focused electron/ion beam applications," *Carbon*, vol. 110, pp. 378–383, 2016.
10. H.-S. Kuo, S. Hwang, T.-Y. Fu, Y.-C. Lin, C.-C. Chang, and T. T. Tsong, "Noble metal/W (111) single-atom tips and their field electron and ion emission characteristics," *Japanese Journal of Applied Physics*, vol. 45, no. 11R, pp. 8972–8983, 2006.
11. L. Swanson and G. Schwind, "A review of the cold-field electron cathode," *Advances in Imaging and Electron Physics*, vol. 159, pp. 63–100, 2009.
12. https://www.hitachi hightech.com/global/science/technical/tech/microscopes/cold_fe/ (accessed April 20, 2020).
13. A. K. Geim and K. S. Novoselov, "The rise of graphene," in *Nanoscience and Technology: A Collection of Reviews from Nature Journals*: World Scientific, pp. 11–19, 2010.
14. D. Ye, S. Moussa, J. D. Ferguson, A. A. Baski, and M. S. El-Shall, "Highly efficient electron field emission from graphene oxide sheets supported by nickel nanotip arrays," *Nano Letters*, vol. 12, no. 3, pp. 1265–1268, 2012.
15. G. Eda, H. Emrah Unalan, N. Rupesinghe, G. A. Amaratunga, and M. Chhowalla, "Field emission from graphene based composite thin films," *Applied Physics Letters*, vol. 93, no. 23, pp. 233502(1)–233502(3), 2008.
16. Z. S. Wu et al., "Field emission of single-layer graphene films prepared by electrophoretic deposition," *Advanced Materials*, vol. 21, no. 17, pp. 1756–1760, 2009.
17. K. S. Novoselov et al., "Two-dimensional gas of massless Dirac fermions in graphene," *Nature*, vol. 438, no. 7065, pp. 197–200, 2005.
18. A. A. Balandin et al., "Superior thermal conductivity of single-layer graphene," *Nano Letters*, vol. 8, no. 3, pp. 902–907, 2008.

19. G. Giovannetti, P. Khomyakov, G. Brocks, V. v. Karpan, J. Van den Brink, and P. J. Kelly, "Doping graphene with metal contacts," *Physical Review Letters*, vol. 101, no. 2, pp. 026803(1)–026809(4), 2008.
20. K. C. Kwon, K. S. Choi, B. J. Kim, J.-L. Lee, and S. Y. Kim, "Work-function decrease of graphene sheet using alkali metal carbonates," *The Journal of Physical Chemistry C*, vol. 116, no. 50, pp. 26586–26591, 2012.
21. X. Shao and A. Khursheed, "A review paper on "Graphene Field Emission for Electron Microscopy"," *Applied Sciences*, vol. 8, no. 6, pp. 868–882, 2018.
22. X. Shao, A. Srinivasan, W. K. Ang, and A. Khursheed, "A high-brightness large-diameter graphene coated point cathode field emission electron source," *Nature Communications*, vol. 9, no. 1, pp. 1–8, 2018.
23. R. D. Young, "Theoretical total-energy distribution of field-emitted electrons," *Physical Review*, vol. 113, no. 1, pp. 110–114, 1959.
24. A. Bahm, G. Schwind, and L. Swanson, "Range of validity of field emission equations," *Journal of Vacuum Science & Technology B: Microelectronics and Nanometer Structures Processing, Measurement, and Phenomena*, vol. 26, no. 6, pp. 2080–2084, 2008.
25. H. Boersch, "Experimentelle Bestimmung der Energieverteilung in thermisch ausgelösten Elektronenstrahlen," *Zeitschrift für Physik*, vol. 139, no. 2, pp. 115–146, 1954.
26. W. Knauer, "Energy broadening in field emitted electron and ion beams," *Optik*, 1981, 59, 335–354.
27. P. Kruit and G. H. Jansen, "Space charge and statistical Coulomb effects," in *Handbook of Charged Particle Optics*: CRC Press, pp. 341–389, 2017.
28. A. Bell and L. Swanson, "Total energy distributions of field-emitted electrons at high current density," *Physical Review B*, vol. 19, no. 7, pp. 3353–3364, 1979.
29. K. H. Loeffler, "Ph.D. thesis," University of Berlin, 1964.
30. B. Cook, T. Verduin, C. Hagen, and P. Kruit, "Brightness limitations of cold field emitters caused by Coulomb interactions," *Journal of Vacuum Science & Technology B, Nanotechnology and Microelectronics: Materials, Processing, Measurement, and Phenomena*, vol. 28, no. 6, pp. C6C74–C6C79, 2010.
31. J. Wiesner and T. Everhart, "Point-cathode electron sources-Electron optics of the initial diode region: Errata and addendum," *Journal of Applied Physics*, vol. 45, no. 6, pp. 2797–2798, 1974.
32. M. Bronsgeest, J. Barth, L. Swanson, and P. Kruit, "Probe current, probe size, and the practical brightness for probe forming systems," *Journal*

of Vacuum Science & Technology B: Microelectronics and Nanometer Structures Processing, Measurement, and Phenomena, vol. 26, no. 3, pp. 949–955, 2008.

33. G. Schwind, G. Magera, and L. Swanson, "Comparison of parameters for Schottky and cold field emission sources," *Journal of Vacuum Science & Technology B: Microelectronics and Nanometer Structures Processing, Measurement, and Phenomena*, vol. 24, no. 6, pp. 2897–2901, 2006.
34. L. Swanson and N. Martin, "Field electron cathode stability studies: Zirconium/tungsten thermal-field cathode," *Journal of Applied Physics*, vol. 46, no. 5, pp. 2029–2050, 1975.
35. L. Swanson, "Current fluctuations from various crystal faces of a clean tungsten field emitter," *Surface Science*, vol. 70, no. 1, pp. 165–180, 1978.
36. P. Blake et al., "Graphene-based liquid crystal device," *Nano Letters*, vol. 8, no. 6, pp. 1704–1708, 2008.
37. N. de Jonge, M. Allioux, J. T. Oostveen, K. B. Teo, and W. I. Milne, "Low noise and stable emission from carbon nanotube electron sources," *Applied Physics Letters*, vol. 87, no. 13, pp. 133118(1)–133118(3), 2005.
38. K. Yeong and J. Thong, "Field-emission properties of ultrathin 5 nm tungsten nanowire," *Journal of Applied Physics*, vol. 100, no. 11, p. 114325, 2006.
39. S. Yamamoto, S. Fukuhara, N. Saito, and H. Okano, "Stabilization of field emission current," *Surface Science*, vol. 61, no. 2, pp. 535–549, 1976.
40. D. Tuggle, L. Swanson, and J. Orloff, "Application of a thermal field emission source for high resolution, high current e-beam microprobes," *Journal of Vacuum Science and Technology*, vol. 16, no. 6, pp. 1699–1703, 1979.
41. N. Saitou, "Trajectory analysis of ions formed in the field emitter inter-electrode region," *Surface Science*, vol. 66, no. 1, pp. 346–356, 1977.
42. H. Todokoro, N. Saitou, and S. Yamamoto, "Role of ion bombardment in field emission current instability," *Japanese Journal of Applied Physics*, vol. 21, no. 10R, pp. 1513–1516, 1982.